A Generalized Constraint Model for Two-Dimensional Beam Flexures: Nonlinear Load-Displacement Formulation

Shorya Awtar[1]
e-mail: awtar@umich.edu

Shiladitya Sen
e-mail: shiladit@umich.edu

Department of Mechanical Engineering,
University of Michigan,
2350 Hayward Street,
Ann Arbor, MI 48109

To utilize beam flexures in constraint-based flexure mechanism design, it is important to develop qualitative and quantitative understanding of their constraint characteristics in terms of stiffness and error motions. This paper provides a highly generalized yet accurate closed-form parametric load-displacement model for two-dimensional beam flexures, taking into account the nonlinearities arising from load equilibrium applied in the deformed configuration. In particular, stiffness and error motions are parametrically quantified in terms of elastic, load-stiffening, kinematic, and elastokinematic effects. The proposed beam constraint model incorporates a wide range of loading conditions, boundary conditions, initial curvature, and beam shape. The accuracy and effectiveness of the proposed beam constraint model is verified by nonlinear finite elements analysis.
[DOI: 10.1115/1.4002005]

1 Introduction

Flexure mechanisms depend on elastic deformations to provide small but smooth and precise motions, and are important elements of machine design [1–8]. Constraint-based design methods are commonly applied to flexure mechanisms because their constituent flexure elements behave like constraints [6–9]. A typical flexure element exhibits relatively small stiffness along certain directions, which may be identified as its degrees of freedom (DoF), and relatively high stiffness along other directions, which act as its degrees of constraint (DoC). Figure 1 provides a comparison between representative traditional and flexure-based constraints that impose a single DoC between two rigid bodies, (1) and (2). The single DoC and associated two DoF, as indicated by the arrows, are realized by: the diameter of the rigid ball and two point contacts in case (A), the length of the rigid link and two traditional hinges in case (B), the length of the rigid link and two lumped-compliance flexure hinges in case (C), and the length of the distributed-compliance flexure beam in case (D).

An ideal constraint should provide zero error motion and infinite stiffness or load-bearing capacity along its DoC directions. Furthermore, it should provide infinite motion range and zero resistance (either stiffness or friction) along its DoF directions. While the traditional elements (A) and (B) come close to this idealization in terms of stiffness, the flexure elements (C) and (D) clearly deviate from ideal constraint behavior. The lumped-compliance flexure element (C) not only provides a relatively large stiffness in the DoC direction but also exhibits a finite stiffness in the two DoF directions resulting in a limited motion range. Compared with (C), distributed-compliance flexure beam (D) offers a relatively lower stiffness in the DoF directions and therefore greater motion range. However, it also exhibits a relatively lower stiffness in the DoC direction, which further drops with increasing

DoF displacements. Moreover, as in the case of the traditional element (B), both flexure elements (C) and (D) exhibit an undesired parasitic error motion along the DoC direction that increases with DoF displacements. These observations qualitatively highlight the following: (1) The nonideal constraint behavior (or performance limitations) of the individual flexure elements in terms of their stiffness and error motions, (2) The tradeoff between DoF and DoC attributes seen in flexure elements, and (3) the differences between the lumped and distributed-compliance geometries, even though both are generally treated as equivalent in the traditional constraint-based design approaches [8,9].

For the purpose of deterministic constraint-based design (i.e., analysis, optimization, and synthesis) of flexure mechanisms, simply identifying the high stiffness directions as DoC and low stiffness directions as DoF is simplistic and inadequate. Instead, a mathematical model that quantifies the constraint behavior of flexure elements in terms of their motion range, error motions, and stiffness is necessary. Furthermore, this model should be closed-form and parametric to allow design insight and optimization and simple enough to be extended to complex flexure mechanism geometries where performance limitations and tradeoffs may not be physically obvious. This goal has been accomplished for a simple (initially straight and uniform thickness) planar beam via the beam constraint model (BCM), as reported previously [7,10,11]. It has been shown that the deviation from ideal constraint behavior and associated performance tradeoffs arise due to the nonlinearity associated with applying load equilibrium in the deformed beam configuration, which can be significant even for small displacements. In addition to the elastic behavior of a flexure beam, the BCM elucidates its load-stiffening, kinematic, and elastokinematic effects in a compact, closed-form, parametric format. Although defined in prior literature, these nonlinear effects are highlighted again in Sec. 2 for the benefit of the reader.

The objective of this paper is to extend the BCM to incorporate further generalizations of a two-dimensional beam in terms of arbitrary end loading and boundary conditions, initial curvature, and thickness variation along the beam length. Such a generalization would encompass, for example, the lumped as well as

---

[1]Corresponding author.
Contributed by the Mechanisms and Robotics Committee of ASME for publication in the JOURNAL OF MECHANICAL DESIGN. Manuscript received October 16, 2009; final manuscript received May 16, 2010; published online August 18, 2010. Assoc. Editor: Ashitava Ghosal.
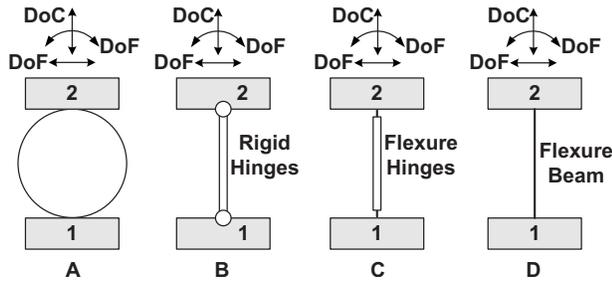
Fig. 1 Comparison of various constraint elements

Fig. 2 Simple beam flexure

distributed-compliance flexure elements (C) and (D) of Fig. 1 under a common constraint model. Section 2 of this paper primes the reader by providing an overview of the previously derived BCM for a simple beam. Section 3 derives the nonlinear load-displacement relations, consistent with the BCM format for a uniform thickness beam with an initial slope and curvature. Section 4 does the same for an initially straight beam with an arbitrarily varying cross-section along its length. This paper concludes in Sec. 5 with a summary of results and plans for future work. All the work presented here is based on a direct load-displacement formulation. An energy-based formulation of the generalized BCM and its application to flexure mechanisms, comprising multiple beam flexures, is reported separately in a follow-up paper [12].

2 Background: The Beam Constraint Model (BCM)

While nonlinearities in beam mechanics have been studied extensively in literature, the challenge here lies in identifying and incorporating only those sources of nonlinearities that are relevant to the constraint behavior of flexure elements. The beam constraint model is based on the *Euler–Bernoulli (E-B) beam theory*, which assumes that plane cross-sections remain plane and perpendicular to the neutral axis after deformation. Although these assumptions are strictly true for long, slender, and uniform cross-section beams under pure moment loading, they are applicable more generally to long and slender beams with variable cross-sections and general loading, for small bending deformations (~10% of beam length) [13]. Moreover, within this deformation range, the beam curvature may be expressed as a linear approximation [13,14]. The moment at a beam cross-section may be determined by either applying load equilibrium in either the undeformed configuration of the beam or, more accurately, in the deformed configuration of the beam. The latter option takes into account the contribution of the axial load to bending moments and along with the linearized curvature approximation leads to a special case of the E-B theory known as *the beam-column theory* [15,16]. The *Timoshenko beam theory* further captures the effect of shear strains in a beam and adds a correction term to the E-B beam equation [17]. While all these beam theories assume small strains, the *finite strain theory* employs the Green strain definition to capture large deformation effects and therefore provides a more general nonlinear beam mechanics formulation [18]. However, for a long, slender, planar beam geometry, this formulation also reduces to the E-B beam theory. In computational mechanics, another generalized nonlinear beam formulation may be derived from the *theory of rods* [19,20], which treats a rod as an assembly of points and associated directors.

Using one or more of the above theories, various analytical models for planar beams have been presented in literature with approximations suitable to their respective applications and deformation range. A sampling of such models is presented here. The Cosserat theory of rods [20], which neglects in-plane or out-of-plane cross-sectional deformations, has been employed to obtain a nonlinear governing equation for prestressed beams [21] that has to be solved numerically given its complexity. The finite strain
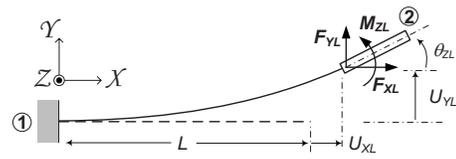
theory has been employed to obtain a nonlinear beam governing equation that includes the effects of in-plane cross-sectional deformations in helicopter rotor blades [22]. Once again, the resulting beam governing equation may only be solved numerically. The E-B beam theory, in it most general form, i.e., with nonlinear curvature and load equilibrium applied in the deformed beam configuration, has been used to model the nonlinearities associated with large deformation of beams [23,24]. The resulting nonlinear beam governing equation may be solved using elliptic integrals [25] for beams with uniform cross-section and specific loading conditions. This approach does not lead to closed-form results and is mathematically too complex for flexure mechanism design.

This concern is addressed to a certain extent by the pseudo-rigid body model (PRBM), which represents a lumped-parameter approach to capturing the large displacement behavior of beam flexures [4,26–28]. However, since the PRBM parameters are obtained via an optimization process that utilizes the exact elliptic integral based solution for a beam, these parameters have to be recomputed for every change in the loading conditions, boundary conditions, or initial beam curvature. Furthermore, for the optimal PRBM to be generated, an exact solution is needed *a priori*, which may not always be possible for a variable cross-section beam. Also, while the PRBM captures load-stiffening and kinematic effects very accurately, its inherent lumped-compliance assumption precludes the elastokinematic effect. Since the elastokinematic effect plays a critical role in determining the DoC direction stiffness, error motions, and performance tradeoffs particularly in distributed-compliance flexures [7,10], the PRBM proves to be inadequate in characterizing their constraint behavior [29].

The E-B beam theory, assuming linearized curvature and load equilibrium applied in the undeformed configuration, yields a linear beam governing equation that may be solved in closed-form to provide the most basic linear elastic model of the beam flexure. This model is obviously inadequate for constraint characterization because it fails to capture the nonlinear load-stiffening, kinematic, or elastokinematic effects.

Since flexure mechanisms typically employ long slender beams that undergo DoF displacements that are within about 10% of the respective beam lengths, the beam curvature nonlinearity is not of much significance (<1% approximation error). However, the presence of an axial or DoC load that can be comparable to the transverse or DoF loads makes the beam-column theory the most suitable basis for the BCM. A brief overview of the BCM for a simple beam flexure (uniform thickness and initially straight) is provided below. For a more detailed mathematical derivation and a discussion of the underlying assumptions, the reader is referred to prior literature [7,10].

Figure 2 illustrates a simple beam (length: L, thickness: T, and depth: H), interconnecting rigid bodies (1) and (2), subjected to generalized end-loads F_{XL}, F_{YL}, and M_{ZL}, resulting in end-displacements U_{XL} (DoC), U_{YL} (DoF), and θ_{ZL} (DoF) with respect to the coordinate frame X-Y-Z. The X direction is also referred to as the axial direction while Y and Θ_Z are frequently referred to as the transverse directions in this paper. I_{ZZ} denotes the second moment of area about the bending axis Z. E denotes the Young's modulus for a state of plane-stress in XY and plate modulus for a state of plane-strain in XY. The *beam governing equation* and associated boundary conditions, resulting from the beam-column theory are as follows:

$$EI_{ZZ}U''_Y(X) = M_{ZL} + F_{YL}(L + U_{XL} - X) - F_{XL}(U_{YL} - U_Y(X))$$

$$\tag{1}$$

$$U_Y(0) = 0, \quad U'_Y(0) = 0, \quad U''_Y(L) = \frac{M_{ZL}}{EI_{ZZ}}$$

$$\text{and} \quad U'''_Y(L) = \frac{-F_{YL} + F_{XL}U'_Y(L)}{EI_{ZZ}} \tag{2}$$

The importance of applying load equilibrium in the deformed configuration of the beam is that while the axial direction load F_{XL} finds a place in this differential equation, the equation itself and associated boundary conditions remain linear in the transverse-direction loads (F_{YL} and M_{ZL}) and displacements ($U_Y(X)$ and its derivatives). Consequently, solving this equation leads to linear relations between these end-loads and end-displacements (U_{YL} and $\theta_{ZL} = U'_{YL}$). However, the associated closed-form stiffness terms are no longer merely elastic but instead are transcendental functions of the axial load F_{XL}. Thus, while the beam governing equation itself is linear in the transverse loads and displacements, nonlinearities associated with the axial load appear in the final end load-displacement relations. These transcendental load-displacement relations are mathematically too complex to offer any qualitative or quantitative insight in flexure mechanism design [30]. Alternate solution approaches either address very specific geometries and loading conditions [31] or require numerical/graphical solution methods [32,33].

In the BCM, we identify a practical load and displacement range of interest, and approximate the abovementioned transcendental relations to yield the following compact and closed-form transverse direction load-displacement relation:

$$\begin{bmatrix} F_{YL}L^2/EI_{ZZ} \\ M_{ZL}L/EI_{ZZ} \end{bmatrix} = \begin{bmatrix} k_{11}^{(0)} & k_{12}^{(0)} \\ k_{12}^{(0)} & k_{22}^{(0)} \end{bmatrix} \begin{bmatrix} \dfrac{U_{YL}}{L} \\ \theta_{ZL} \end{bmatrix} + \frac{F_{XL}L^2}{EI_{ZZ}} \begin{bmatrix} k_{11}^{(1)} & k_{12}^{(1)} \\ k_{12}^{(1)} & k_{22}^{(1)} \end{bmatrix} \begin{bmatrix} \dfrac{U_{YL}}{L} \\ \theta_{ZL} \end{bmatrix}$$

$$\tag{3}$$

This approximation is simply based on an infinite series expansion and truncation of the given transcendental function, which results in less than 1% error for $F_{XL}L^2/EI_{ZZ}$ within ± 5.0. Next, the geometric constraint imposed by the beam arc length is captured via the following integral to determine the dependence of the axial displacement U_{XL} on the transverse displacements:

$$L + \frac{(T/L)^2}{12} \frac{F_{XL}L^2}{EI_{ZZ}} = \int_0^{L+U_{XL}} \left\{ 1 + \frac{1}{2}(U'_Y(X))^2 \right\} dX \tag{4}$$

The left hand side (LHS) and right hand side (RHS) of this equation represent the beam length before and after the deflection, respectively. The undeformed beam length is augmented with any elastic stretch resulting from the axial load F_{XL}, on the LHS. On the RHS, it is important to include the second-order term in $U'_Y(X)$ to capture the kinematics associated the beam's deformed geometry. Using the $U_Y(X)$ solution of Eq. (1), Eq. (4) may also be solved in closed form to reveal a component of U_{XL} that has a quadratic dependence on U_{YL} and θ_{ZL}. As might be expected, the coefficients in this quadratic relation are also transcendental functions of the axial load F_{XL}. Once again, in the BCM a series expansion and truncation to the first power in F_{XL} yields the following axial load-displacement relation with less than 1% error for $F_{XL}L^2/EI_{ZZ}$ within ± 5.0:

Table 1 Characteristic coefficients for a simple beam

$k_{11}^{(0)}$	12	$g_{11}^{(0)}$	$-3/5$
$k_{12}^{(0)}$	-6	$g_{12}^{(0)}$	$1/20$
$k_{22}^{(0)}$	4	$g_{22}^{(0)}$	$-1/15$
$k_{11}^{(1)}$	$6/5$	$g_{11}^{(1)}$	$1/700$
$k_{12}^{(1)}$	$-1/10$	$g_{12}^{(1)}$	$-1/1400$
$k_{22}^{(1)}$	$2/15$	$g_{22}^{(1)}$	$11/6300$

$$\frac{U_{XL}}{L} = \frac{(T/L)^2}{12} \frac{F_{XL}L^2}{EI_{ZZ}} + \begin{bmatrix} \dfrac{U_{YL}}{L} & \theta_{ZL} \end{bmatrix} \begin{bmatrix} g_{11}^{(0)} & g_{12}^{(0)} \\ g_{12}^{(0)} & g_{22}^{(0)} \end{bmatrix} \begin{bmatrix} \dfrac{U_{YL}}{L} \\ \theta_{ZL} \end{bmatrix}$$

$$+ \frac{F_{XL}L^2}{EI_{ZZ}} \begin{bmatrix} \dfrac{U_{YL}}{L} & \theta_{ZL} \end{bmatrix} \begin{bmatrix} g_{11}^{(1)} & g_{12}^{(1)} \\ g_{12}^{(1)} & g_{22}^{(1)} \end{bmatrix} \begin{bmatrix} \dfrac{U_{YL}}{L} \\ \theta_{ZL} \end{bmatrix} \tag{5}$$

Equations (3) and (5) constitute the BCM since they quantify the beam flexure's constraint characteristics, as described further below. In these equations, all loads, displacements, and stiffness terms are naturally normalized with respect to the beam parameters: displacements and lengths are normalized by the beam length L, forces by EI_{ZZ}/L^2, and moments by EI_{ZZ}/L. Thus, one may define

$$\frac{F_{XL}L^2}{EI_{ZZ}} \triangleq f_{x1}; \quad \frac{F_{YL}L^2}{EI_{ZZ}} \triangleq f_{y1}; \quad \frac{M_{ZL}L}{EI_{ZZ}} \triangleq m_{z1}$$

$$\frac{U_{XL}}{L} \triangleq u_{x1}; \quad \frac{U_{YL}}{L} \triangleq u_{y1}; \quad \theta_{ZL} \triangleq \theta_{z1}; \quad \frac{T}{L} \triangleq t; \quad \frac{X}{L} \triangleq x$$

In the rest of this paper, lower-case symbols are used to represent normalized variables and parameters, as per the above convention. It will be shown in Sec. 4 that the stiffness coefficients k's in Eq. (3) and constraint coefficients g's in Eq. (5), in general, are non-dimensional *beam characteristic coefficients* that are solely dependent on the beam shape and not its actual size. For a simple beam, these coefficients take the numerical values listed in Table 1 [7,10,11].

The BCM helps characterize the constraint behavior of a simple beam flexure in terms of its stiffness and error motions. Error motions are the undesired motions of a flexure element or mechanism: any motion in a DoF direction, other than the intended DoF, is referred to as cross-axis coupling, and any motion along a DoC direction is referred to as parasitic error [7]. The first matrix term on the RHS of Eq. (3) provides the linear elastic stiffness in the DoF directions while the second matrix captures load-stiffening, which highlights the change in the effective stiffness in the DoF directions due to a DoC load. Both these matrix terms also capture the cross-axis coupling between the two DoF. Equation (5) shows that the DoC direction displacement, which is a parasitic error motion, comprises three terms. The first term $u_{x1}^{(e)}$ is a purely elastic component resulting from the stretching of the beam neutral axis in the X direction. The second term $u_{x1}^{(k)}$ represents a purely kinematic component dependent on the two DoF displacements and arises from the constant beam arc-length constraint. The third term $u_{x1}^{(e-k)}$ represents an elastokinematic component, called so because of its elastic dependence on the DoC force f_{x1} and its kinematic dependence on the two DoF displacements. The elastokinematic component is also a consequence of the beam arc-length constraint and arises due to a change in the beam deforma-
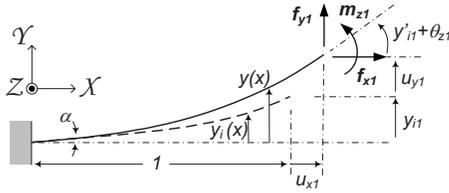
Fig. 3 Initially slanted and curved beam

tion when f_{x1} is applied even as u_{y1} and θ_{z1} are held fixed. The kinematic component $u_{x1}^{(k)}$ dominates the error motion in this DoC direction and increases quadratically with increasing DoF displacements. The elastokinematic component of the DoC displacement while small with respect to the purely kinematic component is comparable to the purely elastic component and causes the DoC direction compliance to increase quadratically from its nominal linear elastic value with increasing DoF displacements.

Thus, the BCM not only highlights the nonideal constraint behavior of a beam flexure, it also reveals interdependence and fundamental tradeoffs between the DoF quality (large range, low stiffness) and DoC quality (high stiffness, low parasitic error). The beam characteristic coefficients serve as convenient performance metrics in a design. The accuracy of the simple beam BCM and its effective application to more complex flexure mechanisms have been demonstrated analytically as well as experimentally in the past [10,29,34].

3 Uniform Thickness Beam With Generalized Boundary Conditions and Initial Curvature

Next, we consider a uniform thickness beam with an arbitrary initial slope and an arbitrary but constant initial curvature. Note that choosing an arbitrary X and Y positions of the beam root simply shifts the coordinate frame of the beam by a constant value and is therefore trivial. The objective here is to capture these initial and boundary condition generalizations within the BCM, which so far has only covered a simple beam. The motivation for doing so is twofold. (1) Analytically capture the consequence of manufacturing variations, e.g., in micro electro-mechanical systems (MEMS), the microfabricated beams can often assume an initially bent/curved shape to relieve material stresses and (2) Use initial slope and curvature as additional design and optimization variables to achieve desired constraint characteristics.

Figure 3 illustrates an initially slanted and curved beam with three generalized end-loads f_{x1}, f_{y1}, and m_{z1}, and three end-displacements u_{x1}, u_{y1}, and θ_{z1}, along the coordinate frame X-Y-Z. All lower-case quantities are normalized with respect to beam parameters, as described earlier. The beam is assumed to have an initial slope α and an initial curvature of κ. For small initial slope and curvature (~ 0.1), the Y and Θ_Z (transverse) directions still serve as DoF, and the X (axial) direction is a DoC. The initial (unloaded and undeformed) beam configuration is denoted by $y_i(x)$, the final (loaded and deformed) beam configuration is given by $y(x)$, and the beam deformation in the Y direction is given by $u_y(x)$, where

$$y_i(x) = \alpha x + \frac{\kappa}{2}x^2 \quad \text{and} \quad y(x) = y_i(x) + u_y(x) \qquad (6)$$

The derivation of the load-displacement relations for this beam flexure is carried out along the same lines as in the case of a simple beam. Euler–Bernoulli and small curvature assumptions are made. The latter requires that the displacement, slope, and curvature of the beam in its deformed configuration remain of the order of 0.1. The normalized bending moment $m_z(x)$ at a given cross section is computed by applying load equilibrium in the beam's deformed configuration:

$$m_z(x) = m_{z1} + f_{y1}(1 + u_{x1} - x) - f_{x1}(y_1 - y(x)) \qquad (7)$$

This leads to the following normalized beam governing equation:

$$y''(x) = m_{z1} + f_{y1}(1 + u_{x1} - x) - f_{x1}(y_1 - y(x)) \implies y^{iv}(x) = f_{x1}y''(x) \qquad (8)$$

For positive values of f_{x1}, the general solution to this fourth-order linear differential equation is given by

$$y(x) = c_1 + c_2 x + c_3 \sinh(rx) + c_4 \cosh(rx) \quad \text{where} \quad r^2 \triangleq f_{x1} \qquad (9)$$

An analogous solution in terms of trigonometric functions, instead of hyperbolic functions, exists for negative values of f_{x1}. The beam deflection, $u_y(x)$, then becomes

$$u_y(x) = y(x) - y_i(x) = c_1 + (c_2 - \alpha x) - \frac{\kappa}{2}x^2 + c_3 \sinh(rx) + c_4 \cosh(rx) \qquad (10)$$

Displacement boundary conditions at the two beam ends are given by

$$u_y(0) = 0, \quad u_y'(0) = 0, \quad u_y(1) = u_{y1}, \quad u_y'(1) = \theta_{z1} \qquad (11)$$

Using Eqs. (6) and (7), the load boundary conditions at $x=1$ can be shown to be

$$u_y'''(1) = -f_{y1} + f_{x1}(\theta_{z1} + \alpha + \kappa), \quad u_y''(1) = m_{z1} \qquad (12)$$

The above displacement and load boundary conditions are then used to determine the constants c_1, c_2, c_3, and c_4, which ultimately lead to the following relations between the DoF direction end-loads and end-displacements:

$$
\begin{bmatrix} f_{y1} \\ m_{z1} \end{bmatrix} =
\begin{bmatrix}
\dfrac{r^3 \sinh(r)}{r \sinh(r) - 2\cosh(r) + 2} & \dfrac{r^2\{1 - \cosh(r)\}}{r \sinh(r) - 2\cosh(r) + 2} \\
\dfrac{r^2\{1 - \cosh(r)\}}{r \sinh(r) - 2\cosh(r) + 2} & \dfrac{r^2 \cosh(r) - r \sinh(r)}{r \sinh(r) - 2\cosh(r) + 2}
\end{bmatrix}
\times \begin{bmatrix} u_{y1} \\ \theta_{z1} \end{bmatrix}
$$
$$
+ \begin{bmatrix}
r^2 & -\dfrac{r^2}{2} \\
0 & \dfrac{4\{\cosh(r) - r\sinh(r) - 1\} + r^2\{1 + \cosh(r)\}}{2\{r \sinh(r) - 2\cosh(r) + 2\}}
\end{bmatrix}
\times \begin{bmatrix} \alpha + \kappa \\ \kappa \end{bmatrix} \qquad (13)
$$

As is expected, setting $\alpha = \kappa = 0$, reduces the above expression to that for a simple beam [10], prior to series expansion and truncation. As earlier, expanding the transcendental functions in the above matrices with respect to r, and truncating its fourth-power or higher terms (or equivalently second-power or higher terms in f_{x1}), provides a great degree of simplification. Over an f_{x1} range of ± 5, the truncation error associated with the first matrix above is less than 1% and with the second matrix is 8%. The simplified DoF direction force-displacement relations may thus be expressed as follows:

$$\begin{bmatrix} f_{y1} \\ m_{z1} \end{bmatrix} = \begin{bmatrix} 12 & -6 \\ -6 & 4 \end{bmatrix} \begin{bmatrix} u_{y1} \\ \theta_{z1} \end{bmatrix} + f_{x1} \begin{bmatrix} \dfrac{6}{5} & -\dfrac{1}{10} \\ -\dfrac{1}{10} & \dfrac{2}{15} \end{bmatrix} \begin{bmatrix} u_{y1} \\ \theta_{z1} \end{bmatrix}$$

$$+ f_{x1} \begin{bmatrix} 1 & -\dfrac{1}{2} \\ 0 & \dfrac{1}{12} \end{bmatrix} \begin{bmatrix} \alpha + \kappa \\ \kappa \end{bmatrix} \tag{14}$$

Fig. 4 DoF force (f_{y1}) versus DoF displacement (u_{y1}) for initially slanted or curved beams

Clearly, the first two terms, in the above matrix equation, are identical to the elastic stiffness and load-stiffening terms, respectively, in Eq. (3) for a simple beam. The last term is new and arises due to the initial slope and curvature. Even though this term might appear similar to the original load-stiffening term, it actually does not change the DoF stiffness values. The presence of α and κ simply shift the DoF load-displacement curves without affecting their slopes. This is corroborated to a high degree of accuracy by means of finite elements analysis (FEA) (see Appendix for details) for three different combinations of α and κ (Fig. 4). The FEA is carried out over a relatively large u_{y1} range (±0.1) with f_{x1} set to 5 and m_{z1} set to 0. This constant shift for the given beam geometry is a consequence of the fact that the DoC load f_{x1} produces additional bending moments along the beam length that are independent of the DoF displacements. The action of this load in the presence of DoF displacements indeed produces load-stiffening but that is captured as usual by the second term in the above expression.

We next proceed to determine the DoC direction load-displacement expression for this flexure beam by imposing the following beam arc-length conservation relation:

$$\int_0^{1+u_{x1}^{(e)}} \left\{ 1 + \frac{1}{2}(y_i'(x))^2 \right\} dx = \int_0^{1+u_{x1}} \left\{ 1 + \frac{1}{2}(u_y'(x) + y_i'(x))^2 \right\} dx \tag{15}$$

The LHS is the total arc length, which is the initial length augmented by the elastic elongation of the beam $u_{x1}^{(e)}$. The RHS computes the total arc length after deformation, and hence the upper limit of integration changes to $(1+u_{x1})$. This DoC direction geometric constraint equation may be solved using the solution for $u_y(x)$ derived earlier in Eq. (10) to yield the following expression for DoC end-displacement:

$$u_{x1} = f_{x1}\frac{t^2}{12} + \begin{bmatrix} u_{y1} & \theta_{z1} \end{bmatrix} \begin{bmatrix} g_{11} & g_{12} \\ g_{21} & g_{22} \end{bmatrix} \begin{bmatrix} u_{y1} \\ \theta_{z1} \end{bmatrix} - \left(\alpha + \frac{\kappa}{2} \right) u_{y1}$$

$$+ g_{33}\left(\frac{\kappa}{2} \right)\theta_{z1} + g_{44}\left(\frac{\kappa}{2} \right)^2 \tag{16}$$

where

$$g_{11} = -\frac{r^2\{\cosh^2(r) + \cosh(r) - 2\} - 3r\,\sinh(r)\{\cosh(r) - 1\}}{2\{r\,\sinh(r) - 2\,\cosh(r) + 2\}^2} \quad \text{where } r^2 \triangleq f_{x1}$$

$$g_{12} = g_{21} = \frac{r^2\{\cosh(r) - 1\} + r\,\sinh(r)\{\cosh(r) - 1\} - 4\{\cosh(r) - 1\}^2}{4\{r\,\sinh(r) - 2\,\cosh(r) + 2\}^2}$$

$$g_{22} = \frac{r^3 - r^2\,\sinh(r)\{\cosh(r) + 2\} + 2r\{2\,\cosh^2(r) - \cosh(r) - 1\} - 2\,\sinh(r)\{\cosh(r) - 1\}}{4r\{r\,\sinh(r) - 2\,\cosh(r) + 2\}^2}$$

$$g_{33} = \frac{r^3\{1 + \cosh(r)\} - r^2\,\sinh(r)\{5 + \cosh(r)\} + 4r\{\cosh^2(r) + \cosh(r) - 2\} - 4\,\sinh(r)\{\cosh(r) - 1\}}{2r\{r\,\sinh(r) - 2\,\cosh(r) + 2\}^2}$$

$$g_{44} = \frac{r^3\{\cosh^2(r) + 3\,\cosh(r) + 2\} - r^2\,\sinh(r)\{7\,\cosh(r) + 11\} + 4r\{4\,\cosh^2(r) + \cosh(r) - 5\} - 12\,\sinh(r)\{\cosh(r) - 1\}}{6r\{r\,\sinh(r) - 2\,\cosh(r) + 2\}^2}$$

Upon setting α and κ to zero, the above DoC direction relation also reduces to the one obtained for a simple beam [10], before series expansion and truncation. Next, as done for the DoF matrix equation, expanding the transcendental constraint terms g's with respect to r (or equivalently f_{x1}) and dropping higher-power terms, provides a considerably more simple and insightful relation:
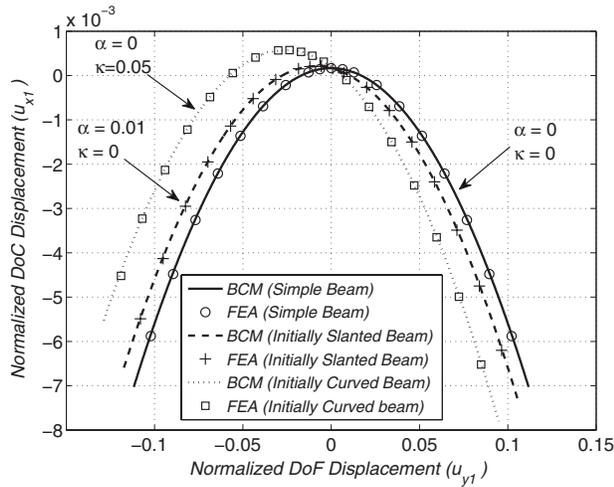
Fig. 5 DoC displacement (u_{x1}) versus DoF displacement (u_{y1}) for initially slanted or curved beams

$$u_{x1} = f_{x1}\frac{t^2}{12} + \{u_{y1} \quad \theta z1\} \begin{bmatrix} -\dfrac{3}{5} & \dfrac{1}{20} \\ \dfrac{1}{20} & -\dfrac{1}{15} \end{bmatrix} \begin{Bmatrix} u_{y1} \\ \theta_{z1} \end{Bmatrix}$$

$$+ f_{x1}\{u_{y1} \quad \theta_{z1}\} \begin{bmatrix} \dfrac{1}{700} & \dfrac{1}{1400} \\ \dfrac{1}{1400} & \dfrac{11}{6300} \end{bmatrix} \begin{Bmatrix} u_{y1} \\ \theta_{z1} \end{Bmatrix}$$

$$- \left(\alpha + \frac{\kappa}{2}\right)u_{y1} - \frac{\kappa}{12}\theta_{z1} + f_{x1}\frac{\kappa}{360}\theta_{z1} + f_{x1}\frac{\kappa^2}{720} \quad (17)$$

The truncation error associated with g_{11}, g_{12}, and g_{22} is less than 1% with g_{33} is less than 3%, and with g_{44} is less than 12%, over an f_{x1} range of ± 5. The first (purely elastic), second (purely kinematic) and third (elastokinematic) terms in the above expression are identical to those obtained for the simple beam (Eq. (5)). The effects of α and κ in the DoC direction are expressed via the last four terms. The fourth and fifth terms contribute extra purely kinematic components. Even though these terms do not exhibit a quadratic dependence on the DoF displacement such as the previous kinematic terms, they are independent of the DoC load. The
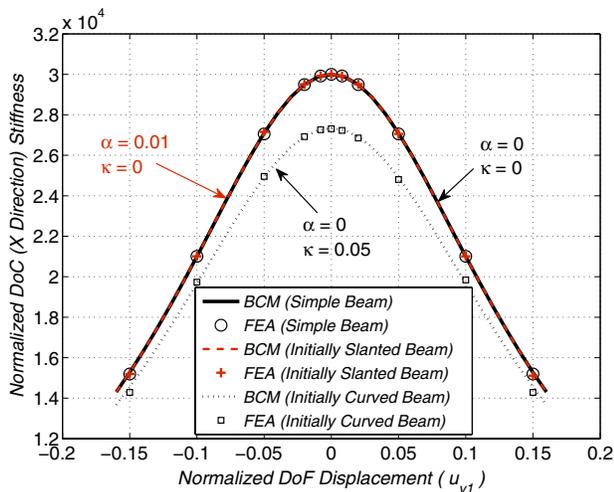
Fig. 6 DoC stiffness versus DoF displacement (u_{y1}) for initially slanted or curved beams
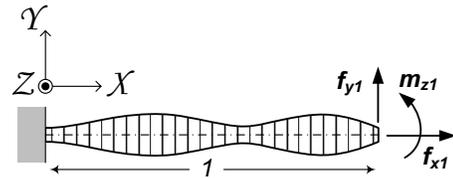
sixth term, which only depends on the initial curvature and not the slant, contributes an extra elastokinematic component, which also is not quadratically dependent on the DoF displacements (u_{y1} and θ_{z1}). However, this term produces a change in the DoC stiffness with increasing θ_{z1} displacement. The seventh and final term in the above expression is a new purely elastic term. Both the sixth and seventh terms arise due to the "uncurling" of the initial beam curvature in the presence of a DoC load f_{x1}. In case of an initially slanted beam with no initial curvature ($\kappa=0$), since this uncurling does not exist, there are no elastic or elastokinematic components when DoF displacements are zero.

These mathematical and physical observations are further verified via FEA for three different combinations of α and κ. Figure 5 plots the parasitic error motion along the X DoC, u_{x1}, against the Y DoF displacement, u_{y1}. The corresponding FEA is carried out with f_{x1} set to 5 and m_{z1} set to 0. Figure 6 plots the X DoC stiffness against the Y DoF displacement, u_{y1}, and the FEA is carried out with θ_{z1} set to 0. The FEA results are all found to be in close agreement with the generalized BCM developed in this section.

Thus, overall, a uniform thickness beam flexure with initial slant and curvature continues to behave like a single DoC constraint element. The constraint characteristics along the DoF direction do not change considerably but the DoC error motion as well as stiffness is influenced by the presence of additional linear, kinematic, and elastokinematic terms. The generalized BCM, given by Eqs. (14) and (17), accurately predicts all these additional terms.

4 Initially Straight Variable Thickness Beams

While in the previous two sections we have considered uniform thickness beams that may be initially straight, initially slanted, and/or initially curved, in this section we attempt a systematic process for developing the BCM for an initially straight beam with any generalized beam cross-sectional variation along its length. Such beam shape variation allows a nonuniform distribution of compliance along the beam length. If the consequence of distributed-compliance is analytically understood in terms of the beam constraint characteristics (stiffness and error motions), one may carry out beam shape optimization.

Figure 7 illustrates an initially straight beam with a varying cross-section in its undeformed configuration subject to three generalized end-loads f_{x1}, f_{y1}, and m_{z1}, along the coordinate frame X-Y-Z. The resulting three end-displacements u_{x1}, u_{y1}, and θ_{z1}, are not shown but are also along the same coordinate frame. The X axis chosen to be along the undeformed neutral axis of the beam. It is also obvious that the Y and Θ_z (transverse) directions still serve as the degrees of freedom while the X (axial) direction is a degree of constraint.

The modeling assumptions remain the same as earlier, except for the fact that I_{zz} is no longer constant and, instead, may be stated as $I_{ZZ}(x) = I_{ZZ0}\xi^3(x)$. I_{ZZ0}, a constant, is the nominal second moment of area and is therefore used in the normalization scheme described earlier. Consequently, the beam governing Eq. (1) becomes

$$\xi^3(x)u_y''(x) = m_{z1} + f_{y1}(1-x) - f_{x1}(u_{y1} - u_y(x)) \quad (18)$$

Given the arbitrariness of the function $\xi(x)$, a straight-forward solution to this ordinary differential equation containing variable

coefficients is no longer possible. Nevertheless, the equation and boundary conditions still remain linear in the transverse loads (f_{y1} and m_{z1}) and displacements ($u_y(x)$). This implies that the resulting relation between the transverse end-loads and end-displacements has to be linear, of the form

$$\begin{Bmatrix} f_{y1} \\ m_{z1} \end{Bmatrix} = \begin{bmatrix} k_{11}(f_{x1};\xi(x)) & k_{12}(f_{x1};\xi(x)) \\ k_{21}(f_{x1};\xi(x)) & k_{22}(f_{x1};\xi(x)) \end{bmatrix} \begin{Bmatrix} u_{y1} \\ \theta_{z1} \end{Bmatrix} \quad (19)$$

The effective stiffness terms (k's) above will now be some complicated functions of the axial load f_{x1} and functionals of the beam shape $\xi(x)$ that may not be known in closed-form. Our strategy here is to simply find the first three terms in the series expansion of these stiffness terms with respect to f_{x1} rather than find the overall function. Based on the previous known cases, it is safe to assume that the contribution of higher-power terms is negligible. Although previously we carried out the expansion of the stiffness terms only to the first power in f_{x1} (Eq. (3)), it has been shown using energy-based arguments [12] that the first-power coefficient (load-stiffening) in the effective stiffness term (k) expansion directly corresponds to the zeroth-power coefficient (kinematic) in constraint term (g) expansion, and similarly the second-power coefficient in the effective stiffness term (k) expansion directly corresponds to the first-power coefficient (elastokinematic) in constraint term (g) expansion. Thus, the complete BCM may be obtained simply working with the above stiffness matrix without the need for separately deriving the constraint matrix using Eq. (4), which is an arduous step. There are two approaches that we take to carry out this strategy for solving Eq. (18)—analytical and numerical. These two approaches are described below along with their respective merits and limitations.

4.1 Analytical Approach. The proposed analytical approach is based on a series solution. Without any loss in generality, the beam shape may be expressed as

$$\xi^3(x) = (b_0 + b_1 x + b_2 x^2 + \ldots + b_n x^n + \ldots) \quad \text{where} \quad b_o \triangleq 1 \quad (20)$$

Next, Eq. (18) is reduced to the following simplified homogenous form by choosing a new independent displacement variable $w(x) = \{m_{z1} + f_{y1}(1-x) - f_{x1}(u_{y1} - u_y(x))\}$:

$$\left(1 + \sum_{i=1}^{\infty} b_i x^i\right) w''(x) = f_{x1} w(x) \quad (21)$$

Since the variable coefficient in this second-order differential equation is an analytic function of x over the range of interest {0 to 1}, it may be solved using the power series solution method [35]. The variable coefficient of $w''(x)$ is never zero because that would mean the second moment of area is zero, which is physically nonviable. Since this coefficient is a polynomial, the solution to the above equation can also be assumed to be an infinite polynomial series as follows:

$$w(x) = a_0 + a_1 x + a_2 x^2 + \ldots + a_n x^n + \ldots = \sum_{n=0}^{\infty} a_n x^n \quad (22)$$

The a's in this expression will be referred to as the *solution coefficients*. Substituting this assumed solution in the homogenized beam governing equation (Eq. (21)) yields

$$\left(1 + \sum_{i=1}^{\infty} b_i x^i\right)\left(\sum_{m=0}^{\infty} \frac{(m+2)!}{m!} a_{m+2} x^m\right) = f_{x1}\left(\sum_{n=0}^{\infty} a_n x^n\right) \quad (23)$$

The above equation is true for all values of x and hence the coefficients of similar powers of x on the RHS and LHS can be equated. To equate the coefficients of the rth power of x on both sides, Eq. (23) is differentiated r times and x is set to zero:

$$\left(\sum_{l=0}^{r}\left[C(r,l)\left\{\frac{d^l}{dx^l}\left(\sum_{i=0}^{\infty} b_i x^i\right)\right\}\right. \right.$$
$$\left. \left. \times \left\{\frac{d^{r-l}}{dx^{r-l}}\left(\sum_{m=0}^{\infty} \frac{(m+2)!}{m!} a_{m+2} x^m\right)\right\}\right]\right)_{x=0}$$
$$= \left(f_{x1}\frac{d^r}{dx^r}\left(\sum_{n=0}^{\infty} a_n x^n\right)\right)_{x=0}$$

$$\Rightarrow \sum_{l=0}^{r}[C(r,l)\{l!(r-l+2)!\}b_l a_{r-l+2}] = f_{x1}a_r r!$$

$$\Rightarrow a_{r+2} = \frac{f_{x1}a_r}{(r+1)(r+2)} - \sum_{p=0}^{r-1}\left\{\frac{(r-p)(r-p+1)}{(r+1)(r+2)}a_{r-p+1}b_{p+1}\right\} \quad (24)$$

This equation relates the coefficient a_{r+2} with all its preceding coefficients, a_0 through a_{r+1}. The variables l, m, n, p, and i are dummy indices used for summation only. Using Eq. (24), the first four coefficients can be calculated to be the following:

$$a_0 = 1.a_0 + 0.a_1, \quad a_1 = 0.a_0 + 1.a_1$$
$$a_2 = \frac{1}{2!}f_{x1}a_0 + 0.a_1, \quad a_3 = -\frac{b_1}{3!}f_{x1}a_0 + \frac{1!}{3!}f_{x1}a_1 \quad (25)$$

From Eq. (25), it may be observed that the initial four coefficients can be all expressed in term of a_0 and a_1. By the method of induction, it is next shown that all a's can be similarly expressed as a linear combination of a_0 and a_1. Let us assume that for some j, each of the coefficients a_2 through a_j is represented in terms of a_0 and a_1:

$$a_n = h_{n,0}a_0 + h_{n,1}a_1 \quad \forall\, 2 \leq n \leq j \quad (26)$$

Substituting Eq. (26) into Eq. (24) with $r+2=j+1$, one may observe that a_{j+1} also turns out in terms of a_0 and a_1:

$$a_{j+1} = \frac{f_{x1}(h_{j-1,0}a_0 + h_{j-1,1}a_1)}{(r+1)(r+2)} - \sum_{i=0}^{j-2}\left\{\frac{(j-i)(j-i-1)}{j(j+1)}h_{j-i,0}b_{i+1}\right\}a_0$$
$$- \sum_{i=0}^{j-2}\left\{\frac{(j-i)(j-i-1)}{j(j+1)}h_{j-i,1}b_{i+1}\right\}a_1 \quad (27)$$

Equation (27) confirms that a_{j+1} can also be expressed in the form of Eq. (26). Thus, by the principle of induction, it is proven that all subsequent a's are of the form of Eq. (26), where $h_{n,0}$ represents the coefficient of a_0 in a_n and $h_{n,1}$ represents the coefficient of a_1 in a_n. Using Eq. (24), the following recursion formula for $h_{n,0}$ and $h_{n,1}$ may be obtained for $n>2$:

$$h_{n,0} = \frac{f_{x1}h_{n-2,0}}{n(n-1)} - \sum_{i=0}^{n-3}\left\{\frac{(n-i-2)(n-i-1)}{n(n-1)}h_{n-i-1,0}b_{i+1}\right\}$$
$$h_{n,1} = \frac{f_{x1}h_{n-2,1}}{n(n-1)} - \sum_{k=0}^{n-3}\left\{\frac{(n-k-2)(n-k-1)}{n(n-1)}h_{n-k-1,1}b_{k+1}\right\} \quad (28)$$

In the above expressions, i and k are dummy variables used simply for summation. Also, it becomes evident that the coefficients $h_{n,0}$ and $h_{n,1}$ are functions of the *beam shape parameters* (b's) and the DoC load f_{x1}. Thus, using Eqs. (22), (26), and (28), the solution for $w(x)$ and $u_y(x)$ may be stated as follows:

$$w(x) = a_0(1 + h_{2,0}x^2 + \ldots + h_{n,0}x^n + \ldots) + a_1(x + h_{2,1}x^2 + \ldots$$
$$+ h_{n,1}x^n + \ldots)$$

$$\Rightarrow u_y(x) = -\frac{1}{f_{x1}}\{m_{z1} + f_{y1}(1 - x)\} + u_{y1}$$

$$+ \frac{1}{f_{x1}}\{a_0 s_0(x) + a_1 s_1(x)\} \quad \text{where}$$

$$s_0(x) \triangleq (1 + h_{2,0}x^2 + \ldots + h_{n,0}x^n + \ldots) \quad \text{and}$$

$$s_1(x) \triangleq (x + h_{2,1}x^2 + \ldots + h_{n,1}x^n + \ldots) \tag{29}$$

The series-solution, given by Eq. (29), is meaningful only when the series is convergent. If the beam shape $\xi^3(x)$ in Eq. (20) is a qth order polynomial, it can be shown that this series-solution is convergent at $x=1$, provided the following convergence criterion is met:

$$\|\text{roots}(\rho^q + b_1\rho^{q-1} + \ldots + b_{q-1}\rho^1 + b_q = 0)\| < 1 \tag{30}$$

The derivation of the above criteria has been reported separately [29]. The displacement solution given by Eq. (29) has two arbitrary constants a_0 and a_1. This is expected since the beam governing equation, Eq. (21), is second-order. The two arbitrary constants are determined by applying the geometric boundary conditions at the fixed end of the beam.

$$u_y(0) = 0, u_y'(0) = 0 \Rightarrow a_0 = m_{z1} + f_{y1} - f_{x1}u_{y1}, a_1 = -f_{y1} \tag{31}$$

Finally, the DoF direction end-load end-displacement relations are obtained by setting $x=1$ in the Eq. (29):

$$u_{y1} = u_y(1), \quad \text{and} \quad \theta_{z1} = u_y'(1)$$

$$\Rightarrow u_{y1}\{f_{x1}s_0(1)\} = f_{y1}(s_0(1) - s_1(1)) + m_{z1}(s_0(1) - 1) \quad \text{and}$$

$$f_{x1}\theta_{z1} + f_{x1}s_0'(1)u_{y1} = f_{y1}(1 + s_0'(1) - s_1'(1)) + m_{z1}s_0'(1) \tag{32}$$

This can be further converted to a matrix format as shown below:

$$f_{x1}\begin{bmatrix} s_0(1) & 0 \\ s_0'(1) & 1 \end{bmatrix}\begin{Bmatrix} u_{y1} \\ \theta_{z1} \end{Bmatrix} = \begin{bmatrix} s_0(1) - s_1(1) & s_0(1) - 1 \\ 1 + s_0'(1) - s_1'(1) & s_0'(1) \end{bmatrix}\begin{Bmatrix} f_{y1} \\ m_{z1} \end{Bmatrix} \tag{33}$$

The above equation is solved to obtain the end-loads in terms of the end-displacements and functions $s_o(x)$ and $s_1(x)$:

$$\begin{Bmatrix} f_{y1} \\ m_{z1} \end{Bmatrix} = \begin{bmatrix} k_{11} & k_{12} \\ k_{21} & k_{22} \end{bmatrix}\begin{Bmatrix} u_{y1} \\ \theta_{z1} \end{Bmatrix}$$

$$\text{where} \quad k_{11} = \frac{f_{x1}s_0'(1)}{\{s_0'(1) - s_1'(1) - s_0(1) + 2\}}$$

$$k_{12} = k_{21} = \frac{f_{x1}\{1 - s_0(1)\}}{\{s_0'(1) - s_1'(1) - s_0(1) + 2\}} \tag{34}$$

$$\text{and} \quad k_{22} = \frac{f_{x1}\{s_0(1) - s_1(1)\}}{\{s_0'(1) - s_1'(1) - s_0(1) + 2\}}$$

Maxwell's reciprocity principle [36], which requires the stiffness matrix to be symmetric, has been employed in going from Eq. (33) to Eq. (34), given the linearity of the beam governing equation established at the beginning of this section. This principle requires the following condition to hold true at all times, and may be used to check the convergence and validity of the solution, as explained later:

$$s_1(1)s_0'(1) - s_0(1)s_1'(1) = -1 \tag{35}$$

The above relation can be easily verified to be true for the simple case in which the variation in cross-section is taken to be zero,

i.e., $\forall b\text{'s}=0$. For this case, the expressions for $h_{n,0}$ and $h_{n,1}$, determined using Eq. (28), are

$$h_{n,0} = \frac{f_{x1}h_{n-2,0}}{n(n-1)}, \quad h_{j,1} = \frac{f_{x1}h_{n-2,1}}{n(n-1)}$$

$$\Rightarrow h_{0,0} = 1, \quad h_{1,0} = 0,$$

$$h_{0,1} = 0, \quad h_{1,1} = 1$$

$$h_{2,0} = \frac{f_{x1}}{2!}, \quad h_{2,1} = 0, \quad h_{3,0} = 0, \quad h_{3,1} = \frac{f_{x1}}{3!} \tag{36}$$

$$h_{4,0} = \frac{f_{x1}^2}{4!}, \quad h_{4,1} = 0, \quad h_{5,0} = 0, \quad h_{5,1} = \frac{f_{x1}^2}{5!}, \quad \text{and so on} \ldots$$

Substituting these values of $h_{n,0}$ and $h_{n,1}$ in Eq. (29), it is observed that the functions $s_0(x)$ and $s_1(x)$ are simply the hyperbolic sine and cosine functions as given below:

$$s_0(x) = \left(1 + \frac{f_{x1}}{2!}x^2 + \frac{f_{x1}^2}{4!}x^4 \ldots\right) = \cosh(\sqrt{f_{x1}}x)$$

$$s_1(x) = \left(x + \frac{f_{x1}}{2!}x^3 + \frac{f_{x1}^2}{2!}x^5 \ldots\right) = \frac{1}{\sqrt{f_{x1}}}\sinh(\sqrt{f_{x1}}x) \tag{37}$$

These values of $s_0(x)$ and $s_1(x)$ satisfy Eq. (35), thus verifying Maxwell's reciprocity principle. One may also check that substituting these hyperbolic functions into the load-displacement relations of Eq. (34) results in the exact transcendental relations for a simple beam [7,10]. Furthermore, the reciprocity principle may be used to determine the number of solution coefficients, a's to be used in Eq. (22). This is equivalent to choosing the highest power of x in $s_0(x)$ and $s_1(x)$ to be retained such that resulting $s_0(1)$ and $s_1(1)$ satisfy Eq. (35) within an acceptable margin of error.

As expected, Eq. (34) confirms the fact that even for a varying cross-section beam the DoF end-loads are linearly related to the DoF end-displacements by a stiffness matrix that is a function of only the DoC force f_{x1} and the beam shape coefficients b's. The final step now is to expand the stiffness terms in Eq. (34) with respect to f_{x1}: the first term (zeroth-power) will provide the elastic stiffness coefficients for the BCM, the second term (first-power) provides the load-stiffening and kinematic coefficients for the BCM, and the third term (second-power) provides the elastokinematic coefficients for the BCM. As discussed earlier, an explicit solution to the constraint Eq. (4) to determine the constraint matrix is not necessary. For reference though, such an explicit derivation has been shown recently [29]. Separately, the purely elastic component of the X DoC displacement is simply given by

$$u_{x1}^{(e)} = f_{x1}\frac{t_0^2}{12}\left\{\int_0^1 \frac{dx}{\xi(x)}\right\} \quad \text{where} \quad t_0 \text{ is the beam thickness at } x = 0 \tag{38}$$

Ultimately, it is seen above that the load-displacement relation format for the variable cross-section beam remains the same as that for the simple beam—only the beam characteristic coefficients change—thus validating the generality of the BCM. The procedure is still closed-form analytical because for a given beam shape, no iterative or numerical methods are required. Furthermore, the beam shape coefficients appear as parameters in the resulting BCM, thus preserving it parametric nature. To recap the analytical approach presented above—the beam shape is first quantified by expressing the second moment of area of the beam as a function of x coordinate and beam shape parameters b's as in Eq. (20). The beam shape parameters are then used to check the convergence criterion given by Eq. (30). Once the convergence criterion is satisfied, the beam shape parameters may be used to calculate the solution coefficients a's in terms of the variables $h_{n,0}$
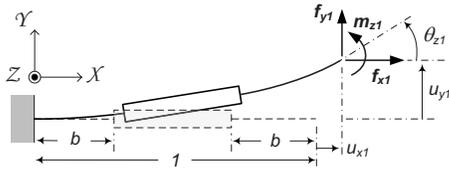
Fig. 8   Variable cross-section beam

and $h_{n,1}$ as per Eq. (28), followed by determination of $s_0(x)$ and $s_1(x)$ as per Eq. (29). The functions $s_0(x)$ and $s_1(x)$ are then truncated in powers of x such that Maxwell's reciprocity criterion, captured by Eq. (35), is satisfied within a certain acceptable error (e.g., 1%) for the given range of problem parameters (DoC force f_{x1} and the beam shape parameters). These functions then provide the stiffness matrix as per Eq. (34). Finally, the resulting stiffness coefficients are expanded in f_{x1} to provide the elastic, load-stiffening, kinematic and elastokinematic coefficients for the BCM.

To validate this approach, it was applied for a flexure beam with the following shape:

$$I_{ZZ}(x) = I_{ZZ0}\{1 + \eta \sin(\pi x)\} \qquad (39)$$

The resulting closed-form parametric BCM, as reported in [29], was verified to be accurate via FEA. However, it is found that the series-solution approach outlined above provides convergence for very small values of η (<0.01). Lack of solution convergence for larger variations that are necessary for the purpose of design and optimization proves to be a serious limitation of this approach. Ongoing work seeks to develop more robust ways for determining and achieving solution convergence. To avoid this limitation, we next propose a numerical approach, which is more effective and powerful but no longer closed-form.

4.2   Numerical Approach. In this subsection, we present a numerical procedure to determine the elastic, load-stiffening, kinematic, and elastokinematic coefficients from Eq. (18). Since this equation contains the end displacement u_{y1}, which is initially unknown, the numerical solution requires an iterative process such that u_{y1} is updated and incrementally corrected at each step.

The algorithm uses numerical values of the beam shape $I_{zz}(x)$ and the end-loads (f_{x1}, f_{y1}, and m_{z1}), along with an initial guess for u_{y1} (=0). For a given end-displacement value $u_{y1}(i)^{in}$ at iteration i, Eq. (18) is solved numerically in MATLAB using ODE45 to output a new value of end-displacement $u_{y1}(i)^{out}$. This new value is then used to update the end-displacement in the next iteration step using a prespecified parameter λ: $u_{y1}(i+1)^{in}=u_{y1}(i)^{in}+\lambda\{u_{y1}(i)^{out}-u_{y1}(i)^{in}\}$. This cycle is repeated until an acceptable convergence is achieved in the u_{y1} value, i.e., the error $u_{y1}(i)^{out}-u_{y1}(i)^{in}$ becomes less than a prespecified parameter ε. At this point, the final values of u_{y1} and u'_{y1} (or θ_{z1}) constitute the desired solution. Parameter λ is chosen to be small enough that the algorithm converges, and large enough so that it converges quickly. A small value of parameter ε ensures the accuracy of the resulting numerical solution. We used $\lambda=0.1$ and $\varepsilon=0.00001$.

Next, in order to solve for the various stiffness terms (k's in Eq. (19), we first determine the analogous compliance coefficients, which are easier to solve for using the above algorithm:

$$\begin{Bmatrix} u_{y1} \\ \theta_{z1} \end{Bmatrix} = \begin{bmatrix} c_{11}(f_{x1};\xi(x)) & c_{12}(f_{x1};\xi(x)) \\ c_{21}(f_{x1};\xi(x)) & c_{22}(f_{x1};\xi(x)) \end{bmatrix} \begin{Bmatrix} f_{y1} \\ m_{z1} \end{Bmatrix} \qquad (40)$$

The following steps are carried out for several discrete numerical values of the DoC force f_{x1}, varied between -5 and $+5$. By setting m_{z1} to 0 and f_{y1} to 1, end-displacements u_{y1} and θ_{z1} provide the numerical values for compliance terms, c_{11} and c_{21}, respectively, for a given value of f_{x1}. Similarly, by setting m_{z1} to 1 and f_{y1} to 0, end-displacement u_{y1} and θ_{z1} give the compliance terms
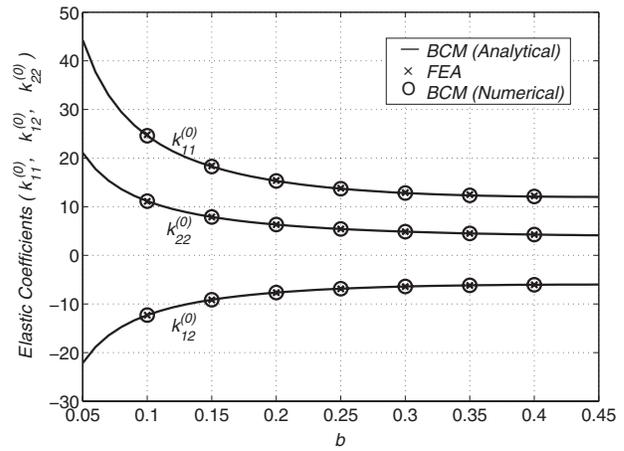
Fig. 9   Elastic stiffness coefficients: BCM versus FEA

c_{12} and c_{22}, for the same given value of f_{x1}. Numerical values of the stiffness coefficients for this given value f_{x1} are then simply found by inverting the above compliance matrix.

Having carried out the above step for several discrete values of f_{x1}, each of the stiffness coefficients k_{11}, $k_{12}=k_{21}$, and k_{22}, is expressed as a high order polynomial function of f_{x1}, using curve fitting techniques, as shown below:

$$\begin{bmatrix} k_{11}(f_{x1}) & k_{12}(f_{x1}) \\ k_{21}(f_{x1}) & k_{22}(f_{x1}) \end{bmatrix} = \begin{bmatrix} k_{11}^{(0)} & k_{12}^{(0)} \\ k_{12}^{(0)} & k_{22}^{(0)} \end{bmatrix} \begin{Bmatrix} u_{y1} \\ \theta_{z1} \end{Bmatrix} + f_{x1} \begin{bmatrix} k_{11}^{(1)} & k_{12}^{(1)} \\ k_{12}^{(1)} & k_{22}^{(1)} \end{bmatrix} \begin{Bmatrix} u_{y1} \\ \theta_{z1} \end{Bmatrix}$$
$$+ f_{x1}^2 \begin{bmatrix} k_{11}^{(2)} & k_{12}^{(2)} \\ k_{12}^{(2)} & k_{22}^{(2)} \end{bmatrix} \begin{Bmatrix} u_{y1} \\ \theta_{z1} \end{Bmatrix} + \ldots \qquad (41)$$

As per the strategy described in the beginning of this section, only the first three terms in the above polynomial are needed for completing the BCM. Thus, using this numerical procedure, which is completely automated, the BCM for a beam with any type of varying cross-section can be found. The approach is not limited by convergence issues and is applicable to considerably large shape variations, as long as Eq. (18) and its underlying assumptions remain valid.

Next, we illustrate the application of this method to a specific case of beam shape generalization, shown in Fig. 8. The beam flexure in this case comprises two uniform thickness compliant portions, each of length b, separated by a rigid portion in the middle. The beam shape is completely determined by parameter b: $b=1/2$ represents the simple beam with uniformly distributed compliance while $b\rightarrow 0$ corresponds to a lumped-compliance to-
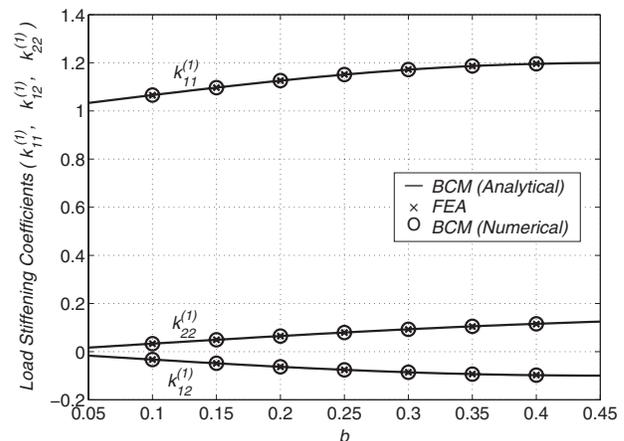
Fig. 10   Load stiffening coefficients: BCM versus FEA
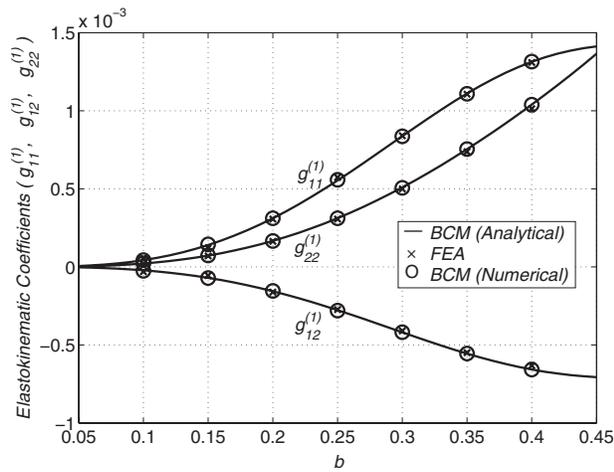
Fig. 11 Elastokinematic coefficients: BCM versus FEA

pology. Given the relative simplicity of this shape, closed-form parametric BCM can be derived for this beam and has been reported previously [10,11]. These closed-form results, along with nonlinear FEA, are used here to verify the effectiveness and accuracy of the proposed numerical approach in Fig. 9 (elastic stiffness coefficients), Fig. 10 (load-stiffening coefficients), and Fig. 11 (elastokinematic coefficients).

These figures show that the numerically derived BCM lies within a 1% deviation from the FEA as well as closed-form BCM. The numerical BCM derivation and FEA can be carried out only for discrete values of the beam shape parameter b, which was varied from 0.1 to 0.4 in increments of 0.05 in this study. It should be noted that as the compliant portions of the beam become shorter, i.e., b approaches 0, the Euler–Bernoulli assumption of plane-section remaining plane becomes weaker and a Timoshenko correction factor is needed to maintain accuracy [17]. Although this correction factor has not been included in the BCM presented above, this may be readily done without additional mathematical complexity.

The proposed numerical approach was also applied to other more complicated beam shapes including $I_{zz}(x)=I_{zzo}(1+\eta \sin(\pi x))$ and $I_{zz}(x)=I_{zzo}(1+\eta \sin^2(\pi x))$ with η as large as 2. In each case, the resulting numerical BCM was found to agree with nonlinear FEA within less 2% error.

We conclude this section with some comments on the closed-form and parametric nature of BCM for variable cross-section beams. For specific beam shape generalizations, such as shown in Fig. 8, the BCM can be derived in a closed-form such that the beam shape parameter(s) appear in the model [10,11] without the need for any iterative or numerical procedures. Any change in parameters such end-loads, end-displacements, or beam shape (b) does not require a rederivation of the entire model. For a greater generalization in the beam shape, a series based analytical approach is presented and is found to be accurate, when it converges. In this case also, there is no iteration involved and the BCM can be derived in closed-form. However, this approach poses convergence problems for beam shape variations that are large enough to be of practical value. The numerical approach, on the other hand, is capable of handling any possible beam shape as well as large variations without any convergence issues. However, determining the beam characteristic coefficients in the BCM requires numerical as well as iterative procedures. Therefore, the model is no longer closed-form or parametric with respect to the beam shape. Despite this, the numerical approach is a useful tool for gaining design insight and performing design optimization.

5 Conclusion

The BCM is a dimensionless, compact, closed-form, and parametric mathematical model of the constraint characteristics of a beam flexure with generalized end-loads and boundary conditions. It is based on the beam-column theory (linearized curvature and load equilibrium applied in deformed configuration) and assumes normalized displacements and loads within ± 0.1 and ± 5.0, respectively. Within this range, it captures the relevant nonlinear effects (load-stiffening, kinematic, and elastokinematic) to accurately predict the error motions and stiffness properties of a beam flexure.

While the BCM for a simple beam has been reported in the past, the key contribution of this paper is to further generalize the BCM to include beams with any initial slope/curvature and any variable cross-sectional shape. The resulting generalized BCM brings a wide range of beam shapes and geometries under a common constraint characterization scheme. The objective of this effort is to provide a qualitative and quantitative basis for systematic constraint-based design that recognizes and leverages the deviations of flexure elements from ideal constraint behavior. The ability to vary the beam initial slant, initially curvature, or beam shape to achieve desired constraint characteristics by means of geometric optimization is an important first step in this direction.

It is important to point out that, in addition to the constraint characteristics (stiffness and error motions) described here, other considerations such as maximum stress levels, material selection, manufacturing and assembly, integration of sensors and actuators, etc., also have to be taken into account in an overall design and optimization process, depending on the application. In particular, stresses are not explicitly included as part of the BCM and are only indirectly reflected in the stiffness predictions.

Finally, the formulation presented here is based on the direct application of load equilibrium and geometric constraint conditions for each individual beam flexure. An energy-based formulation of the BCM has been derived and separately presented [12] so that it may be applied to the modeling, analysis, and optimization of flexure mechanisms, comprising complex arrangements of flexure beams, in a mathematically more efficient manner.

Appendix: Summary of FEA Parameters

The closed-form analytical expressions for the initially slanted/curved beam and the variable cross-section beams are validated by means of nonlinear finite element analysis performed in ANSYS. BEAM4 elements are used with consistent matrix and large displacement options turned on and shear coefficients set to zero. The material assumed is Stainless Steel, and typical values for Young's Modulus ($210,000$ N mm^{-2}) and Poisson's ratio (0.3) are used. Beam length (L)=250 mm, thickness (T)=5 mm, and height (H)=50 mm are employed with each beam flexure meshed using 300 BEAM4 elements. The convergence criterion for all cases is set to 0.001 relative tolerance limit on the L2 norm calculated on forces.

References

[1] Jones, R. V., 1988, *Instruments and Experiences: Papers on Measurement and Instrument Design*, Wiley, New York, NY.
[2] Smith, S. T., 2000, *Flexures: Elements of Elastic Mechanisms*, Gordon and Breach, New York.
[3] Slocum, A. H., 1992, *Precision Machine Design*, Society of Manufacturing Engineers, Dearborn, MI.
[4] Howell, L. L., 2001, *Compliant Mechanisms*, Wiley, New York, NY.
[5] Lobontiu, N., 2003, *Compliant Mechanisms: Design of Flexure Hinges*, CRC, Boca Raton, FL.
[6] Hale, L. C., 1999, "Principles and Techniques for Designing Precision Machines," Ph.D. thesis, Massachusetts Institute of Technology, Cambridge MA.
[7] Awtar, S., 2004, "Analysis and Synthesis of Parallel Kinematic XY Mechanisms," Sc.D. thesis, Massachusetts Institute of Technology, Cambridge, MA.
[8] Blanding, D. K., 1999, *Exact Constraint: Machine Design Using Kinematic Principles*, ASME, New York, NY.
[9] Hopkins, J. B., 2005, "Design of Parallel Systems via Freedom and Constraint

Topologies (FACT)," MS thesis, Massachusetts Institute of Technology, Cambridge, MA.

[10] Awtar, S., Slocum, A. H., and Sevincer, E., 2007, "Characteristics of Beam-Based Flexure Modules," ASME J. Mech. Des., **129**(6), pp. 625–639.

[11] Awtar, S., and Sevincer, E., 2006, "Elastic Averaging in Flexure Mechanisms: A Multi-Parallelogram Flexure Case-Study," Proc. ASME IDETC/CIE 2006, Philadelphia, PA, Paper No. 99752.

[12] Awtar, S., and Sen, S., 2010, "A Generalized Constraint Model for Two-Dimensional Beam Flexures: Nonlinear Strain Energy Formulation," ASME J. Mech. Des., **132**, p. 081009.

[13] Crandall, S. H., Dahl, N. C., and Lardner, T. J., 1972, *An Introduction to the Mechanics of Solids*, McGraw-Hill, New York.

[14] Srinath, L. S., 1980, *Advanced Mechanics of Solids*, Tata McGraw-Hill, New Delhi.

[15] Krylov, A. N., 1931, *Calculation of Beams on Elastic Foundation*, Russian Academy of Sciences, St. Petersburg.

[16] Timoshenko, S. P., 1956, *Strength of Materials Part II*, D. Van Nostrand, Princeton.

[17] Timoshenko, S. P., 1921, "On the Correction Factor for Shear of the Differential Equation for Transverse Vibrations of Bars of Uniform Cross-Section," Philos. Mag., **41**, pp. 744–746.

[18] Novozhilov, V. V., 1953, *Foundations of the Nonlinear Theory of*, Elasticity, Graylock, Rochester, NY.

[19] Green, A. E., and Laws, N., 1966, "A General Theory of Rods," Proc. R. Soc. London, Ser. A, **293**(1433), pp. 145–155.

[20] Rubin, M. R., 2000, *Cosserat Theories: Shells, Rods and Points*, Springer, New York.

[21] Lacarbonara, W., Paolone, A., and Yabuno, H., 2004, "Modeling of Planar Nonshallow Prestressed Beams Towards Asymptotic Solutions," Mech. Res. Commun., **31**(3), pp. 301–310.

[22] Hodges, D. H., and Dowell, E. H., 1974, "Nonlinear Equations of Motion for the Elastic Bending and Torsion of Twisted Nonuniform Rotor Blades," NASA Tech. Note D-7818.

[23] Bisshopp, K. E., and Drucker, D. C., 1945, "Large Deflection of Cantilever Beams," Q. Appl. Math., **3**(3), pp. 272–275.

[24] Frisch-Fay, R., 1963, *Flexible Bars*, Butterworth, Washington, DC.

[25] Mattiasson, K., 1981, "Numerical Results From Large Deflection Beam and Frame Problems Analyzed by Means of Elliptic Integrals," Int. J. Numer. Methods Eng., **17**, pp. 145–153.

[26] Howell, L. L., and Midha, A., 1995, "Parametric Deflection Approximations for End-loaded, Large-Deflection Beams in Compliant Mechanisms," ASME J. Mech. Des., **117**(1), pp. 156–165.

[27] Howell, L. L., and Midha, A., 1996, "Parametric Deflection Approximations for an Initially-Curved, Large-Deflection Beams in Compliant Mechanisms," Proc. ASME DETC 1996, MECH-1215.

[28] Howell, L. L., Midha, A., and Norton, T. W., 1996, "Evaluation of Equivalent Spring Stiffness for Use in a Pseudo-Rigid Body Model of Large-Deflection Compliant Mechanisms," ASME J. Mech. Des., **118**(1), pp. 126–131.

[29] Awtar, S., and Sen, S., 2009, "A Generalized Constraint Model for Two-Dimensional Beam Flexures," Proc. ASME IDETC/CIE 2009, San Diego, CA, Paper No. 87808.

[30] Plainevaux, J. E., 1956, "Etude des deformations d'une lame de suspension elastique," Nuovo Cimento, **4**, pp. 922–928.

[31] Legtenberg, R., Groeneveld, A. W., and Elwenspoek, M., 1996, "Comb-Drive Actuators for Large Displacements," J. Micromech. Microeng., **6**, pp. 320–329.

[32] Haringx, J. A., 1949, "The Cross-Spring Pivot as a Constructional Element," Appl. Sci. Res., **1**(1), pp. 313–332.

[33] Zelenika, S., and DeBona, F., 2002, "Analytical and Experimental Characterization of High Precision Flexural Pivots Subjected to Lateral Loads," Precis. Eng., **26**, pp. 381–388.

[34] Awtar, S., and Slocum, A. H., 2007, "Constraint-Based Design of Parallel Kinematic XY Flexure Mechanisms," ASME J. Mech. Des., **129**(8), pp. 816–830.

[35] Simmons, G. F., and Robertson, J. S., 1991, *Differential Equations With Applications and Historical Notes*, H. McGraw, ed., pp. 176–181.

[36] Reddy, J. N., 2002, *Energy Principles and Variational Methods in Applied Mechanics*, 2nd ed., Wiley, New York, p. 164.